

High-power picosecond fiber source for coherent Raman microscopy

Khanh Kieu,^{1,†} Brian G. Saar,^{2,†} Gary R. Holtom,² X. Sunney Xie,^{2,3} and Frank W. Wise^{1,4}

¹Department of Applied Physics, Cornell University, Ithaca, New York 14853, USA

²Department of Chemistry and Chemical Biology, Harvard University, Cambridge, Massachusetts 02138, USA

³xie@chemistry.harvard.edu

⁴fwise@ccmr.cornell.edu

Received March 3, 2009; revised April 23, 2009; accepted May 15, 2009;
posted May 26, 2009 (Doc. ID 108323); published June 29, 2009

We report a high-power picosecond fiber pump laser system for coherent Raman microscopy (CRM). The fiber laser system generates 3.5 ps pulses with 6 W average power at 1030 nm. Frequency doubling yields more than 2 W of green light, which can be used to pump an optical parametric oscillator to produce the pump and the Stokes beams for CRM. Detailed performance data on the laser and the various wavelength conversion steps are discussed, together with representative CRM images of fresh animal tissue obtained with the new source. © 2009 Optical Society of America

OCIS codes: 140.3510, 180.4315, 190.4380.

Picosecond or femtosecond pulsed laser sources are preferred for a wide variety of multiphoton microscopy techniques, such as two-photon-excited fluorescence [1], second-harmonic generation (SHG) [2], coherent anti-Stokes Raman scattering (CARS) [3,4], and stimulated Raman scattering (SRS) [5]. For these applications, the laser source ideally should be tunable, provide watt-level average power, and have the ability to precisely tailor the temporal properties of the pulse to the application. Mode-locked solid-state lasers based on titanium:sapphire are perhaps the most widely used in multiphoton microscopy, because they satisfy all of these requirements. However, these free space lasers are costly and require precise mechanical alignment and vibrational isolation for good performance.

Coherent Raman microscopy (CRM) offers label-free optical imaging with chemical contrast based on intrinsic molecular vibrational frequencies in the sample. For CRM techniques, which include CARS and SRS, the ideal pulse duration is a compromise: shorter pulses offer high peak power (and therefore signal) but limited spectral resolution, while longer pulses generate less signal but with better spectral resolution and specificity [4]. In practice, picosecond excitation is preferred to match the spectral width of the laser source to the intrinsic linewidth of molecular vibrational frequencies ($\sim 15 \text{ cm}^{-1}$ or $\sim 1 \text{ nm}$ at 800 nm). In addition, synchronized pulses of two colors, at least one of which must be tunable, are necessary and fairly high average powers are required, because the excitation optical path has limited total throughput (typically $\sim 10\%$ including the microscope) and powers in the range of 10–100 mW are applied to the sample [4]. The pulse trains can be generated with synchronized mode-locked Ti:sapphire lasers [6], for example. An alternate approach is to employ a solid-state laser to synchronously pump an optical parametric oscillator (OPO) that generates the two colors [7].

Fiber lasers offer attractive properties for this application, including permanent optical alignment, good beam quality, and potentially low cost. A fiber-

based source for coherent Raman microspectroscopy was reported by Andresen *et al.* [8]. This instrument supplies picosecond and femtosecond pulses and has the valuable property of being environmentally stable. However, its output power needs to be increased by at least 1 order of magnitude for rapid imaging.

Here we describe an integrated fiber source of high-energy transform-limited picosecond pulses. The 1030 nm pulses from the fiber source are frequency doubled, and the resulting pulses at 515 nm are used to pump an OPO, which provides tunable two pulse trains that can be used for CARS imaging. Compared with picosecond solid-state lasers currently in use for CRM [7], the fiber source described here offers shorter pulses, is air cooled, and is compact. It is a first step toward an all-fiber source of pulses for use in CARS imaging.

The primary challenge in the design of the high-power picosecond-pulsed source is the control of nonlinear effects. In the context of CRM, the dominant concern is that nonlinearity will broaden the spectrum, which degrades the spectral resolution. Established approaches to the mitigation of nonlinear effects in fiber amplifiers include chirped-pulse amplification (CPA) and self-similar amplification [9], but neither of these is well suited to the parameters needed for CRM. CPA with picosecond pulses generally requires impractically large dispersion to stretch the pulse. In self-similar amplification, the spectral bandwidth increases, so extremely narrow-band input pulses would be needed. A direct amplification technique is therefore more appropriate.

The picosecond-pulsed source (Fig. 1) includes an oscillator, a preamplifier, and a main amplifier. The amplifier is designed to optimize efficiency and pulse quality by the choice of fiber length and core diameters and by the use of cladding pumping with a novel fiber combiner.

The first stage of the system is a soliton oscillator based on established techniques. It incorporates a semiconductor saturable-absorber mirror (SESAM) and a chirped fiber Bragg grating (CFBG) for anoma-

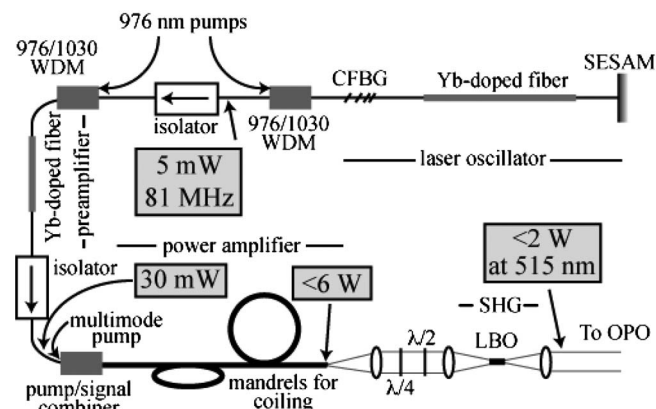


Fig. 1. Schematic of the picosecond laser system. Output power levels after each stage are indicated in gray boxes. Also shown is the LBO crystal used for SHG. WDM, wavelength division multiplexer; $\lambda/2$, $\lambda/4$, half- and quarter-wave plates, respectively.

lous dispersion. The oscillator generates 5 mW of ~ 3.5 ps soliton pulses at 81 MHz repetition rate. The CFBG provides large anomalous dispersion (approximately -5 ps²) and has 50% reflectivity in its 2 nm (full width at half maximum) reflection bandwidth. The narrow reflection bandwidth effectively filters out the spectral sidebands that generally occur in soliton mode locking. This is necessary to avoid subsequent preferential amplification of the sidebands. The SESAM is glued to the polished end of the fiber so the oscillator is alignment free. With this design, stable and self-starting mode-locked operation is easily achieved. The spectrum and the intensity autocorrelation from the oscillator are shown in Figs. 2(a) and 2(b), respectively.

Pulses from the oscillator are preamplified in a standard single-mode gain fiber. The preamplifier gain is limited to about 6 to avoid nonlinear effects. The spectral bandwidth and the pulse duration are unchanged after the preamplifier stage. The preamplifier could be eliminated if the oscillator were optimized to give higher output power.

Cladding pumping of the main amplifier is required to reach average powers of several watts. With the highest available doping levels, approximately 1 m of gain fiber is needed to absorb most of the pump light. The gain fiber has 20 μ m core and 125 μ m cladding diameters. The small cladding diameter enables large pump absorption per length (about 30 dB/m at 976 nm), which helps to reduce the length of the gain fiber. The main amplifier stage consists of 90 cm of the gain fiber coiled at ~ 7.5 cm diameter in two orthogonal planes to filter higher-order modes [10]. A

pump/signal combiner fabricated in our laboratory is part of the gain fiber segment. A tapered multimode fiber for the pump light is fused to a single-mode fiber, which is then spliced to the double-clad gain fiber. The core of the single-mode fiber is expanded to ensure good coupling to the lowest-order mode of the multimode gain fiber. Thus, the structure integrates pump/signal beam combining with a mode-field adapter in a relatively short segment, which reduces the nonlinear phase accumulation that can distort the pulse.

With up to 14 W of pump power, up to 6 W is obtained from the amplifier. The beam quality is good; $M^2=1.1$ is measured. The spectra of the amplified pulses at different output powers are shown in Fig. 2(c). For powers above ~ 2 W the spectrum begins to distort. At 6 W the spectrum has broadened by about four times and developed a dip in the center. The pulse duration does not change, but the pulses become chirped. Moderate spectral broadening is tolerable, because it does not translate into spectrally broadened pulses after SHG (see below). Good pulse-to-pulse stability was observed ($<1\%$ fluctuations), and the laser could operate for hours without adjustment.

Frequency doubling of the 1030 nm output of the fiber amplifier is carried out using noncritical phase matching in a 20 mm lithium triborate (LBO) crystal. Results are shown in Fig. 3. Structure in the second-harmonic spectrum changes with the incident fundamental power [Fig. 3(a)], but the overall bandwidth is constrained by the phase-matching bandwidth of the LBO crystal to ~ 1 nm. As the input power increases, the harmonic spectrum narrows, and by comparing with Fig. 2(c) we conclude that spectral broadening in the fiber amplifier pushes energy outside the phase-matching bandwidth. As a result, the harmonic power increases less than quadratically with fundamental power [Fig. 3(c)], but the efficiency ($\sim 30\%$) is still reasonable. For second-harmonic power near 1 W, the 2.7 ps pulse duration [Fig. 3(b)] is close to the transform limit.

The frequency-doubled output of the fiber amplifier is used to pump an OPO. The singly resonant OPO (Levante Emerald, APE GmbH) employs a 20 mm LBO crystal for noncritically phase-matched parametric generation. With 1.1 W pump power [corresponding to the intermediate spectra of Figs. 2(c) and 3(a)], the total power from the OPO is 550 mW in the signal and the idler waves, for approximately 50% conversion efficiency. The signal wave is continuously tunable in the range of 740–1005 [Fig. 4(a)]. The sig-

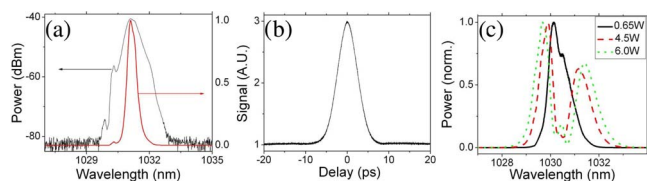


Fig. 2. (Color online) (a) Optical spectrum of the laser oscillator. (b) Intensity autocorrelation of the pulses from the oscillator. (c) Optical spectra of the pulses at the output of the amplifier at the indicated power levels.

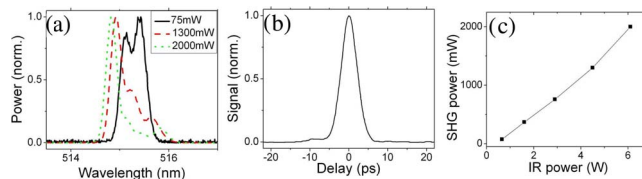


Fig. 3. (Color online) (a) Spectra of the pulses after frequency doubling. (b) Background-free autocorrelation of the green pulses at ~ 1 W average power. (c) SHG power versus fundamental power.

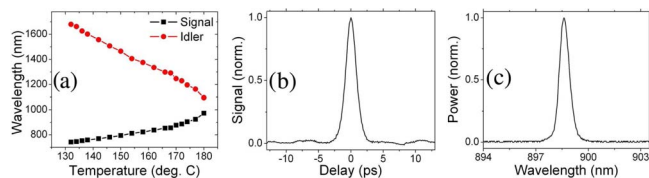


Fig. 4. (Color online) (a) Temperature tuning curve of the OPO (signal wavelength is measured and idler wavelength is calculated). (b) Background-free autocorrelation of the signal output near 900 nm. (c) Optical spectrum of the signal wave.

nal pulses are typically 1.5 ps in duration [Fig. 4(b)], while the spectral bandwidth is 0.7 nm or about 9 cm^{-1} at 900 nm [Fig. 4(c)]. The time-bandwidth product is 0.4, which is very close to the transform limit. The final pulse duration is approximately half that of the fiber amplifier, as expected given the use of two quadratic nonlinear processes with small group-velocity mismatches. It is almost ideal; for CRM imaging, the ratio of resonant (chemically specific) signal/total CARS signal increases with longer pulses but saturates between 1 and 2 ps for a typical Raman band [6], exactly the regime in which this system operates.

To produce CARS images, the signal and the idler outputs of the OPO are tuned into resonance with the CH_2 stretching frequency that is commonly used to image lipids ($\lambda_{\text{signal}} = 898.4\text{ nm}$, $\lambda_{\text{idler}} = 1206.8\text{ nm}$). The combined beams are directed into a laser scanning microscope (Olympus BX62WI/FV300) and focused onto the sample. The focal spot is scanned and the CARS signal is detected by a nondescanned photomultiplier tube positioned behind filters, which pass only the anti-Stokes wavelength ($\lambda_{\text{anti-Stokes}} = 715.5\text{ nm}$).

Figure 5(a) shows a CARS image in the *stratum corneum* obtained from the surface of fresh mouse skin tissue. The image highlights the lipid-rich intercellular space between corneocytes. Figure 5(b) shows the cells of the oil-rich sebaceous gland and

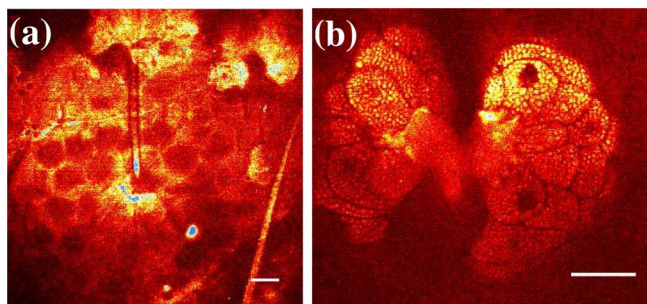


Fig. 5. (Color online) CARS images: (a) CARS image at the CH_2 stretching frequency (2845 cm^{-1}) showing the lipid distribution in the *stratum corneum* of wild-type mouse skin. (b) CARS image of the lipid distribution in the sebaceous gland $30\text{ }\mu\text{m}$ deep in tissue. Scale: $20\text{ }\mu\text{m}$.

demonstrates subcellular resolution at a depth of $30\text{ }\mu\text{m}$ below the surface of the tissue. The large dark areas are the nuclei of the individual cells. These images are comparable in resolution and signal-to-noise ratio to previous images taken with solid-state laser sources [3] and were acquired with a total average power of $\sim 35\text{ mW}$ at the sample (three times lower than in the previous paper, which used 6–7 ps pulses) and with a scanning speed of one frame per second with five-frame averaging. The threefold reduction in power was possible because of the increased efficiency of signal generation using shorter pulses.

In conclusion, we have demonstrated a practical high-power picosecond fiber source for CRM. The frequency-doubled output of the fiber amplifier pumps an OPO to generate widely tunable and narrow-linewidth signal and idler waves. CARS images obtained with this source illustrate the potential of fiber lasers for CRM. Future work will address better control of nonlinearity in the picosecond source along with the development of all-fiber sources of tunable pulses.

Support for this work was provided by the National Institutes of Health (NIH) (grant EB002019 to F. W. Wise), the National Science Foundation (NSF) (grant DBI-0649892 to X. S. Xie), and the Department of Energy (DOE) (grant DE-FG02-07ER64500 to X. S. Xie). B. G. Saar was supported by the United States Army Research Office (USARO) through a National Defense Science and Engineering Graduate fellowship. We thank C. Freudiger for helpful discussions.

[†]Each author contributed equally to this work.

References

- W. Denk, J. H. Strickler, and W. W. Webb, *Science* **248**, 73 (1990).
- P. J. Campagnola, M.-d. Wei, A. Lewis, and L. M. Loew, *Biophys. J.* **77**, 3341 (1999).
- C. L. Evans, E. O. Potma, M. Puoris'haag, D. Côté, C. P. Lin, and X. S. Xie, *Proc. Natl. Acad. Sci. USA* **102**, 16807 (2005).
- C. L. Evans and X. S. Xie, *Annu. Rev. Anal. Chem.* **1**, 883 (2008).
- C. W. Freudiger, W. Min, B. G. Saar, S. Lu, G. R. Holtom, C. He, J. C. Tsai, J. X. Kang, and X. S. Xie, *Science* **322**, 1857 (2008).
- E. O. Potma and X. S. Xie, in *Handbook of Biomedical Nonlinear Optical Microscopy*, B. R. Masters and P. T. C. So, eds. (Oxford U. Press, 2008), p. 412.
- F. Ganikhanov, S. Carrasco, X. S. Xie, M. Katz, W. Seitz, and D. Kopf, *Opt. Lett.* **31**, 1292 (2006).
- E. R. Andresen, C. K. Nielsen, J. Thøgersen, and S. R. Keiding, *Opt. Express* **15**, 4848 (2007).
- M. E. Fermann, V. I. Kruglov, B. C. Thomsen, J. M. Dudley, and J. D. Harvey, *Phys. Rev. Lett.* **84**, 6010 (2000).
- J. P. Koplow, D. A. V. Kliner, and L. Goldberg, *Opt. Lett.* **25**, 442 (2000).